Simulated Road Profiles According to ISO 8608 in Vibration Analysis

Article *in* Journal of Testing and Evaluation · January 2018

DOI: 10.1520/JTE20160265

1 author:

Peter Múčka
Slovak Academy of Sciences
61 PUBLICATIONS **729** CITATIONS

SEE PROFILE

MÚČKA, P., "Simulated road profiles according to ISO 8608 in vibration analysis," In Journal of Testing and Evaluation, ISSN 0090-3973, Vol. 46, 2018, No. 1, pp. 405-418.

doi: 10.1520/JTE20140493

Publisher: ASTM International

Peter Múčka*

Simulated Road Profiles According to ISO 8608 in Vibration Analysis

ABSTRACT

Nowadays, synthetic longitudinal road profiles based on an ISO 8608 road classification are used for simulation purposes to solve various tasks in vibration analysis of mechanical and civil structures and road-vehicle-driver interaction system. Standard ISO 8608 specifies road classification of longitudinal road profiles based on vertical displacement power spectral density (PSD). PSD represented on logarithmic scales is characterized by two parameters of a straight line, an unevenness index and waviness. The aim of this study was to compare spectrum parameters of real roads with ISO 8608 road classes used in scientific papers. Road classes that were used in a sample of 27 current scientific papers were analyzed. Results often indicated marked differences among road classes used for simulation purposes in comparison to the spectrum properties of real roads. For simulation purposes, road class A may be recommended as representative of typical good or average quality road (motorway, expressway, and first class road). Classes B and C may be appropriate to simulate low-quality paved surfaces (2nd and 3rd class roads or local highways).

Keywords: vibration, vehicle, road profile, power spectral density, waviness, ISO 8608.

Introduction

Simulated longitudinal random road profiles are a useful tool often used for vibration analysis of various mechanical and civil structures. Typical example of using such profiles is to evaluate vehicle vibration response:

- to optimize vehicle or seat suspension;
- to estimate energy harvesting and regeneration in a vehicle suspension;
- to evaluate dynamic load of pavement or vehicle;
- to control vibration in a mechanical structure, and;
- to solve various tasks of bridge-vehicle dynamics.

Standard ISO 8608 [1] specifies the road classification of longitudinal random road profiles based on vertical displacement power spectral density (PSD). The statistical road profile description specified in ISO 8608 can be used for one- or two track computer and laboratory road simulation [2,3]. A PSD-based approach is widely used in automotive engineering. Road elevation PSD is applied in the development process of a vehicle or vehicle parts in the frequency domain as well as in the time domain [4]. Various methods of Gaussian and non-Gaussian random vibration testing for automobile application were addressed in [5–11].

Many researchers currently use road classes specified in ISO 8608 [1]. The ISO 8608 standard does not specify a correlation of road class with a road category or with a road quality. Road classes are based on measurements provided mostly in the 60s and 70s. Smoothness level of roads was probably lower 40–50 years ago. Further, a sample size of test sections measured in the 60s and 70s was limited. Braun et al. [12] processed about 30 and La Barre [13] 53 test sections.

ISO 8608 does not specify verbally defined categories of road classes such as very good (Class A), good (Class B), average (Class C), etc. The predecessor of ISO 8608 was the British Standard Institution (BSI) proposal [14] that assigned verbal categories to road classes. These verbal categories are often used without any correlation to a smoothness level of current road network.

* Research Worker, Institute of Materials and Machine Mechanics, Slovak Academy of Sciences, Dúbravská cesta 9, SK-84513 Bratislava 4, Slovak Republic. Email: ummsmuc@savba.sk

It should be interesting to determine the correlation between ISO road classes used in scientific papers and road spectrum properties of real road profiles. Profiles of a large amount of the road network were measured and processed in the last 10-20 years and these results were not considered in ISO road classification. Imprudent use of ISO road classes for simulation purposes may lead to excessive expectations and unrealistic results.

The objectives of this study were as follows:

- Summarize use of ISO 8608 road classes in current scientific literature;
- Summarize road spectrum parameters for real roads based on current measurements;
- Compare results for real roads with used ISO 8608 road classes;
- Estimate the correlation between road elevation spectrum parameters; and
- Suggest recommendations on using ISO 8608 road classes.

Road Classification According to ISO 8608

Measured longitudinal road profile, i.e., a vertical displacement of a road profile in a longitudinal direction, $h(l)$, where h (m) is road elevation dependent on distance l (m) along the track, is considered to be a realization of a random function $H(l)$. Provided that this function is centred, homogeneous, and Gaussian, it is fully described by its power spectral density $G_d(\Omega)$ (m^3/rad), where Ω (rad/m) ($\Omega = 2\pi/L$, L is wavelength) is the angular spatial frequency [1,15,16]. Longitudinal unevenness is the deviation of a longitudinal profile from a straight reference line in a wavelength range of 0.5 m to 50 m according to the definition in prEN 13036-5 [16].

Simplest analytical expression of road elevation PSD has a form [1,16]

$$G_d(\Omega) = G_d(\Omega_0)(\Omega/\Omega_0)^{-w} \tag{1}$$

where $G_d(\Omega_0)$ (m^3/rad) is unevenness index, w is waviness and Ω_0 (rad/m) is reference angular spatial frequency. ISO 8608 defines the fitting interval of a raw PSD by a straight line in angular spatial frequency range from 0.069 rad/m to 17.77 rad/m, i.e., in a wavelength band, L = 0.3534–90.9 m. Eq 1 represents a line on a log-log chart with $G_d(\Omega_0)$ as the vertical ordinate at reference angular spatial frequency Ω_0 and w as the slope of the line (Fig. 1). Parameters $G_d(\Omega_0)$ and w are independent. While $G_d(\Omega_0)$ is proportional to road elevation variance, w expresses a wavelength distribution between particular spatial frequency bands. Waviness $w = 2$ presents the case when the change of the road vertical displacement per unit distance travelled, i.e. road velocity PSD ($G_v(\Omega)$), corresponds to white-noise signal and $G_v(\Omega)$ is the constant, $G_v(\Omega) = G_v(\Omega_0) = G_d(\Omega)\Omega^2$. Estimation of parameters $G_d(\Omega_0)$ and w from a measured road profile $h(l)$ is defined in ISO 8608 and prEN 13036-5 standards. Road roughness classification according to $G_d(\Omega_0)$ is proposed for waviness $w = 2$ in ISO 8608 and prEN 13036-5 standards. Note, that various denotations are used for parameter $G_d(\Omega_0)$ such as unevenness index, roughness coefficient, roughness index, roughness exponent, or degree of roughness.

Straight-line approximation (in a log-log scale) of road elevation PSD based on measurements of real roads was introduced in the 60s [12,13,17] and later was implemented in ISO 8608 and prEN 13036-5. Andrén [15] presented an exhaustive overview of analytical approximations of PSD.

The BSI proposal [14] was the predecessor of ISO 8608. That proposal was published in 1972 and classification was based on a sample of 53 test sections of a length 0.4–35 km. The BSI proposal [14] assumed a road elevation spectrum approximation with two straight lines with different waviness values, $w_1 = 2$ and $w_2 = 1.5$ and break frequency, $n_0 = 1/2\pi$ cycles/m (i.e., $\Omega_0 = 1$ rad/m, $L_0 = 6.28$ m). Waviness values were corrected to $w_1 = 3$ and $w_2 = 2.25$ in Robson [18]. The BSI proposal [14] stated that in general terms motorways are of type A or B. Principal roads may cover a range A to D and minor roads lie in a range from C to E. Unsurfaced roads fall in the lower end of class E.

Two-line spectrum approximation [14] with reference spatial frequency, n_0, may be written as follows:

$$G_d(n) = \begin{cases} G_d(n_0)(n/n_0)^{-w_1} & 0 < n \le n_0 \\ G_d(n_0)(n/n_0)^{-w_2} & n_0 \le n < \infty \end{cases} \tag{2}$$

Using unevenness index for road management is popular in some European countries such as Germany, the UK, Russia, or Czech Republic. These classifications assumed mostly a constant waviness $w = 2$.

ISO 8608 specifies road classification based on unevenness index $G_d(\Omega_0)$ or $G_d(n_0)$. Road classification enables consideration of a road profile in particular octave bands because the PSD is not always a straight line. The constant waviness $w = 2$ is assumed. Waviness $w = 2$ has an advantage as a very easy simulation of

a road profile by integrating white noise. Road classifications according to ISO 8608 and BSI proposal are presented in Table 1.

Table 1. Road classification according to the BSI proposal [14] and ISO 8608 [1]

Road class	BSI proposal				ISO 8608			
	$G_d(n_0)$ (10^{-6} m^3/cycles), $n_0 = 1/2\pi$ cycles/m $w_1 = 2$, $w_2 = 1.5$		$G_d(\Omega_0)$ (10^{-6} m^3/rad), $\Omega_0 = 1$ rad/m $w_1 = 2$, $w_2 = 1.5$		$G_d(\Omega_0)$ (10^{-6} m^3/rad) $\Omega_0 = 1$ rad/m $w = 2$		$G_d(n_0)$ (10^{-6} m^3/cycles) $n_0 = 0.1$ cycles/m $w = 2$	
	Range	Geometric mean	Range	Geometric mean	Range	Geometric mean	Range	Geometric mean
A	2–8	4	0.32–1.27	0.64	< 2	1	< 32	16
B	8–32	16	1.27–5.1	2.55	2–8	4	32–128	64
C	32–128	64	5.1–20.4	10.2	8–32	16	128–512	512
D	128–512	256	20.4–81.5	40.7	32–128	64	512–2048	1024
E	512–2048	1024	81.5–326	163	128–512	256	2048–8192	4096
F	—	—	—	—	512–2048	1024	8192–32768	16384
G	—	—	—	—	2048–8192	4096	32768–131072	65536
H	—	—	—	—	> 8192	16384	> 131072	262144

Following conversion relationship holds between $G_d(\Omega_0)$ and $G_d(n_0)$

$$G_d(\Omega_0)\ (\text{m}^3/\text{rad}) = G_d(n_0)/2\pi\ (\text{m}^3/\text{cycles}) \tag{3}$$

For two alternative reference spatial frequencies, $\Omega_0 = 1$ rad/m and $n_0 = 0.1$ cycles/m, the following conversion for $w = 2$ holds

$$G_d(n_0) = 2\pi G_d(\Omega_0)[\Omega_0/(2\pi n_0)]^w = 15.91 G_d(\Omega_0) \sim 16 G_d(\Omega_0) \tag{4}$$

Examples of simulated road profiles are shown in Fig. 1(a). Profiles correspond to the mean values of A to D classes and their PSDs are shown in Fig. 1(b).

Current Use of ISO 8608 Road Classes

In the current literature, road classes are mostly defined for reference angular spatial frequency $\Omega_0 = 1$ rad/m ($L_0 = 6.28$ m), for angular frequency, $n_0 = 1/2\pi$ cycles/m ($L_0 = 6.28$ m) or $n_0 = 0.1$ cycles/m ($L_0 = 10$ m).

Table 2 shows an overview of spectrum parameters used in 27 randomly selected current scientific papers [19–45]. Because of different reference frequencies, the data were converted to $G_d(\Omega_0)$ with using Eqs 3 and 4 in the fifth column of Table 2. Data in Table 2 show that 59% (16/27) of processed papers used class A, 67% (18/27) class B, 67% (18/27) class C, 37% (10/27) class D, 33% (9/27) class E, 30% (8/27) class F, 7% (2/27) class G, and 4% (1/27) class H. Road class C or higher classes were used by 70% (19/27) authors and class D or higher classes by 41% (10/27) authors.

Some authors [23,29,34,45] still use the BSI proposal. The percentage of such papers can be estimated at 10–20 %.

Papers often addressed various tasks for bridge-vehicle dynamics [19,30,36–38,40,41], energy harvesting and regeneration in vehicle suspension system or in a civil engineering structure [22,24,28,36] or vehicle suspension optimization [20,21,24,25,27,46].

Using unrealistic road classes may lead to great or misleading expectations. For example, Zuo and Zhang [34] investigated the energy harvesting potential of a vehicle suspension system and obtained a RMS power of one shock absorber 14.6 W based on in-situ measurement. Using B and C classes led to a calculated RMS power of 40 and 160 W. Xie and Wang [22] calculated for an energy harvester structure excited by class B, a value of RMS power of about 738 W.

Table 2. Overview of ISO road classes used in current scientific literature.

#	Reference	$G_d(n_0)$ (10^{-6} m^3/cycles)	n_0 (cycles/m)	$G_d(\Omega_0)$ (10^{-6} m^3/rad), Ω_0 = 1 rad/m	ISO 8608 road classes	Application of road classes
1	Aied, Gonzáles, and Cantero [19]	4, 96, 1536	0.1	0.25, 6, 96	A, C, E	Structural deterioration of bridge construction
2	Shen et al. [20]	5	0.1	0.31	A	Improved design of dynamic vibration absorber
3	Ataei et al. [21]	64	1/2π	10.2	C	Multi-objective optimization of hybrid electromagnetic suspension system
4	Xie and Wang [22]	64, 256, 1024	0.1	4, 16, 64	B, C, D	Developing of a dual-mass piezoelectric bar harvester
5	Prendergast, Hester, and Gavin [23]	4, 16, 64, 256, 1024 Note: w_1 = 3, w_2 = 2.25 (Eq 2)	1/2π	0.6, 2.5, 10.2, 40.7, 163	A to E	Damage detection in bridges using vibration-based method
6	Huang et al. [24]	16, 64, 256, 1024	0.1	1, 4, 16, 64	A to D	Developing and optimization of vehicle suspension system with energy harvesting capability
7	Drehmer, Paucar Casas, and Gomes [25]	16, 64, 256, 1024, 4096, 16384	0.1	1, 4, 16, 64, 257, 1029	A to G	Optimization of vehicle suspension
8	Xiao and Zhu [26]	256, 1024	0.1	16, 64	C, D	Design of quarter-car active suspension system
9	Wang et al. [27]	64	0.1	4	B	Optimization of vibration control strategy for a vehicle's active suspension
10	Zhang, Cai, and Deng [28]	5, 20, 80, 256, 1280	1/2π	0.8, 3.2, 12.7, 40.7, 204	A to E	Piezoelectric-based energy harvesting on bridge
11	Reza-Kashyzadeh et al. [29]	4, 16, 64, 256, 1024 Note: w_1 = 2, w_2 = 1.5 (Eq 2)	1/2π	0.6, 2.5, 10.2, 40.7, 163	A to E	Influence on transfer function of passive and semi active suspension system of a quarter-car model
12	Jaksic, O'Connor, and Pakrashi [30]	6, 16, 64, 256, 1024	1/2π	1, 2.5, 10.2, 40.7, 163	A to E	Damage detection in a bridge deck with consideration of bridge-vehicle interaction
13	Zhou et al. [31]	16, 262144	0.1	1, 16470	A, H	Signal analysis of seismic signals to identify the structure differences of wheel and track based on quarter-car model response
14	Oliva et al. [32]	16, 256	0.1	1, 16	A, C	Method for modeling dynamic interaction between road vehicles and bridges
15	Shiiba, Obana, and Machida [33]	16, 64, 256, 1024	0.1	1, 4, 16, 64	A to D	Performance of a real-time multibody dynamics simulation using linearized constraint equations
16	Zuo and Zhang [34]	16, 64	1/2π	2.5, 10.2	B, C	Energy harvesting potential in the vehicle model suspension system
17	Li et al. [35]	64, 256, 1024, 4096	0.1	4, 16, 64, 257	B to E	Relationship between anti-rollover stability and the vehicle lateral stability
18	Zhang, Cao, and Yu [36]	64	0.1	4	B	Design of active and energy-regenerative controllers for the DC-motor-based suspension
19	González, O'Brien, and McGetrick [37]	16	0.1	1	A	Proposal of a novel method for the identification of the damping ratio of a bridge using acceleration measurements from a moving vehicle
20	Chang, Wu, and Zang [38]	16, 64, 256	0.1	1, 4. 16	A to C	Analyses of vehicle–bridge interaction using a rigid disk wheel model

21	Harris et al. [39]	8, 16, 64, 128, 256	0.1	0.5, 1, 4, 8, 16	A to C	Proposal of a novel method for the characterization of pavement roughness through an analysis of vehicle accelerations
22	González et al. [40]	1, 4, 8, 16, 32	1/2π	0.2, 0.6, 1.3, 2.5, 5.1	A, B	Influence of speed and distance between vehicles on the bridge dynamic response
23	Ding, Hao, and Zhu [41]	3.1, 12.6, 50.3, 201.1	1/2π	0.5, 2, 8, 32	A to C	Developing of evolutionary spectral method to evaluate the dynamic vehicle loads on bridges
24	Xu and Wong [42]	64	0.1	4	B	Quantifying traffic-induced building vibration in a stochastic way
25	Yarmohamadi and Berbyuk [43]	19.5, 319.2, Note: $w = 3$	1/2π	3.1, 50.8	A, E	Simulation of kinematic and dynamic properties (comfort, handling) of truck with individual front suspension and rigid front axle
26	Chen et al. [44]	32, 128, 512, 2048	0.1	2, 8, 32, 128	A to D	Estimation of ride comfort and ride safety in vehicle-road dynamic interaction system
27	Reina and Delle Rose [45]	64 Note: $w_1 = 2$, $w_2 = 1.5$ (Eq 2)	1/2π	10.2	C	Estimation of attenuation of mechanical vibrations in automotive suspensions using active vibration absorbers

Road Classes and Maximum Vehicle Velocity

Different vehicle velocities were used for vibration response simulation on the same road classes. Some authors took into account poor road quality and used a lower velocity. Huang et al. [24] used four classes of A to D but considered limited velocity when travelling over poorer-quality roads. They used velocity $v = 120$ km/h for class A, 50 km/h for class C and 30 km/h for class D. Xiao and Zhu [26] assumed road classes C and D and $v = 7$ km/h. Some authors used too high velocity for poor-quality roads. Zhang, Cai and Deng [28] used seven different vehicle speeds ranging from 30 to 120 km/h for A to E road classes. Jaksic, O'Connor, and Pakrashi [30] used velocity range of 10–150 km/h for A to E classes. Reza-Kashyzadeh et al. [29] used $v = 70$ km/h for classes A to E.

In reality it could be dangerous to drive a rough profile at a higher velocity. Recommended maximum vehicle velocity was estimated based on vehicle mathematical model and threshold values of ride comfort and ride safety measures. A simple quarter-car model (Fig. 2) was used with following parameters: unsprung mass, $m_1 = 34.5$ kg, sprung mass, $m_2 = 230$ kg, tire spring radial stiffness, $k_1 = 150{,}190$ N/m, suspension spring coefficient, $k_2 = 14{,}559$ N/m, and suspension damping coefficient, $b_2 = 1380$ Ns/m. Parameters corresponds to the reference quarter-car model ('golden car' model) that is used for estimation of International Roughness Index [47,48].

Equations of motion of the quarter-car model vertical vibration are as follows:

$$\begin{aligned} m_1\ddot{z}_1 + b_2(\dot{z}_1 - \ddot{z}_2) + k_2(z_1 - z_2) + k_1(z_1 - h) = 0 \\ m_2\ddot{z}_2 + b_2(\dot{z}_2 - \dot{z}_1) + k_2(z_2 - z_1) = 0 \end{aligned} \quad (5)$$

where z_1 and z_2 are vertical displacements of unsprung mass m_1 (wheel) and spung mass m_2 (vehicle body), $\dot{z}_1$ and $\dot{z}_2$ are vertical velocities, $\ddot{z}_1$ and $\ddot{z}_2$ are vertical accelerations and h is vertical displacement of road profile.

Ride comfort was quantified with RMS value of frequency-weighted acceleration of the sprung mass (σ_{a2w}) based on ISO 2631-1: 1997 [49]. The filter W_k intended for the vertical acceleration on the seat surface was used for simulation.

Ride safety was quantified with dynamic load coefficient (DLC). DLC is a coefficient of variation of vertical tire force. DLC is defined as a ratio of RMS value of vertical dynamic tire force (σ_{Fdyn}) and vertical static tire force (F_{stat}) as follows: $\mathrm{DLC} = \sigma_{Fdyn} / F_{stat}$. Time-variable dynamic tire force $F_{dyn}(t)$ is a product of tire radial stiffness, k_1, and axle vertical stroke as follows, $F_{dyn}(t) = k_1(z_1 - h)$. The static tire force was calculated as $F_{stat} = (m_1 + m_2)g = 2.595$ kN, where g is the gravitational acceleration ($g = 9.81$ m/s^2).

Threshold values of ride comfort and ride safety was considered as follows:

(a) Ride comfort – ISO 2631-1 [49] presents "likely reactions" of passengers in a public transport. The range of RMS values of frequency-weighted vertical acceleration on the seat surface is defined as follows: < 0.315 m/s^2 (not uncomfortable), 0.315–0.63 m/s^2 (a little uncomfortable), 0.5–1 m/s^2 (fairly uncomfortable), 0.8–1.6 (uncomfortable), 1.25–2.5 m/s^2 (very uncomfortable), > 2 m/s^2 (extremely uncomfortable). Lower limit of 'very uncomfortable' category, σ_{a2w} = 1.25 m/s^2, was chosen as a threshold.

(b) Ride Safety – DLC levels are not standardized. DLC ranges from 0.01 to 0.4 in reality [50]. A DLC value above 0.3 is considered to be a very high. Value of DLC = 0.3 was chosen as ride safety threshold [50,51]. Extreme values of dynamic axle load could be estimated to be $F_{\mathrm{dynmax}} = 3\sigma_{\mathrm{Fdyn}}$ [50].

Quarter-car model vibration response was calculated in frequency domain. RMS value of frequency-weighted acceleration of the sprung mass, σ_{a2w}, was calculated as follows:

$$\sigma_{\mathrm{a2w}}^2 = \int_{f_{\mathrm{m}}}^{f_{\mathrm{M}}} G_{\mathrm{a2w}}(f)\,df = \int_{f_{\mathrm{m}}}^{f_{\mathrm{M}}} |W_k(f)|^2 |H_{\mathrm{a2}}(if)|^2 G_d(f)\,df \tag{6}$$

where $G_{\mathrm{a2w}}(f)$ is PSD of frequency-weighted acceleration of the sprung mass, $H_{\mathrm{a2}}(if)$ is the frequency response function between the road profile vertical displacement, h, and sprung mass acceleration, $\ddot{x}_2$, and is defined as follows

$$H_{\mathrm{a2}}(i\omega) = \frac{b_2 k_1 (i\omega)^3 + k_1 k_2 (i\omega)^2}{m_1 m_2 (i\omega)^4 + b_2 (m_1 + m_2)(i\omega)^3 + (m_1 k_2 + m_2 (k_1 + k_2))(i\omega)^2 + b_2 k_1 (i\omega) + k_1 k_2} \tag{7}$$

where ω (rad/s) is angular frequency ($\omega = 2\pi f$) and i is imaginary unit.

Road elevation PSD as a function of frequency f can be expressed as $G_d(f)$ [m^{2}s] = $(2\pi/v)G_d(\Omega)$ [m^3/rad]. The integration limits in relation (6) were set between f_{m} = 0 Hz and f_{M} = 50 Hz. Contribution of the frequency band above 25 Hz is negligible. This integration interval covers both quarter-car model natural frequencies: sprung mass bounce, f_1 = 1.2 Hz, and unsprung mass bounce, f_2 = 10.3 Hz.

RMS value of dynamic tire force, σ_{Fdyn}, was calculated as follows:

$$\sigma_{F_{\mathrm{dyn}}}^2 = \int_{f_{\mathrm{m}}}^{f_{\mathrm{M}}} G_{F_{\mathrm{dyn}}}(f)\,df = \int_{f_{\mathrm{m}}}^{f_{\mathrm{M}}} \left|H_{F_{\mathrm{dyn}}}(if)\right|^2 G_d(f)\,df\,, \tag{8}$$

where f (Hz) is temporal frequency, $G_{F_{\mathrm{dyn}}}(f)$ is PSD of the dynamic tire force, $H_{F_{\mathrm{dyn}}}(if)$ is the frequency response function between the road profile vertical displacement, h, and dynamic tire force, $G_{\mathrm{d}}(f)$ is the road profile PSD. The transfer function $H_{F_{\mathrm{dyn}}}(i\omega)$ has the form

$$H_{F_{\mathrm{dyn}}}(i\omega) = \frac{m_1 m_2 k_1 (\mathrm{i}\omega)^4 + (m_1 + m_2) b_2 k_1 (\mathrm{i}\omega)^3 + (m_1 + m_2) k_1 k_2 (\mathrm{i}\omega)^2}{m_1 m_2 (\mathrm{i}\omega)^4 + b_2 (m_1 + m_2)(\mathrm{i}\omega)^3 + (m_1 k_2 + m_2 (k_1 + k_2))(\mathrm{i}\omega)^2 + b_2 k_1 (\mathrm{i}\omega) + k_1 k_2} \tag{9}$$

Fig. 3 shows dependence of the quarter-car model vibration response on velocity as a function of ISO 8608 road classes. Limits of maximum vehicle model velocity are summarized in Table 3 as a function of upper limit of particular road class and ride comfort and ride safety thresholds. Theoretical results indicated that ISO road classes A and B are appropriate for higher traversing velocities typical for motorways, expressways, and first class roads, road class C for velocities typical for secondary roads (~30–60 km/h), and class D is suitable for velocities below < 15 km/h. These estimations are limited due to using a simple linear vehicle model with one set of parameters. Results in Table 3 provide only basic insight into the relation between ISO road classes and vehicle velocity.

Table 3. Recommended maximum vehicle model velocity as a function of ISO 8608 road classes

ISO 8608 road class	A	B	C	D	E
Upper limit value of ISO 8608 road class: $G_d(\Omega_0)$ (m^3/rad)	2	8	32	128	512
v_{MAX} (km/h) for ride comfort threshold value, $a_{2\mathrm{w}}$ = 1.2 m/s^2	> 100	> 100	~ 31	~ 8	~ 3
v_{MAX} (km/h) for ride safety threshold value, DLC = 0.3	> 100	> 100	~ 59	~ 15	~ 4

Unevenness Index of Real Road Sections

Table 4 presents statistics of a calculated unevenness index based on 9 different sources. For data published in Andrén [15] and Kollmer et al. [51], the values were roughly estimated from figures.

Table 4. Statistics of unevenness index of real road sections.

Source	Road surface type/ Road functional category	Length (km)	Number of sections	$G_d(\Omega_0)$ (10^{-6} m^3/rad) Ω_0 = 1 rad/m					
				mean	std	min	max	P5	P95
Kawamura and Kaku [61]	Various – Summer	–	10	0.63	0.57	0.06	1.72	–	–
	Various – Winter	–	10	4.01	7.73	0.82	25.94	–	–
Braun and Hellenbroich [54]	Total	1282	12820	1.68	3.57	0.29	62.2	0.4	4.5
	AC surfaces	882.5	8826	1.78	4.17	0.30	62.2	0.43	4.88
	PCC surfaces	399.4	3994	1.46	1.57	0.29	18.1	0.4	3.45
	Highways	–	240	1.0	–	0.3	7.8	–	–
	Federal roads	–	70	2.1	–	0.4	9.5	–	–
	Country roads	–	35	5.3	–	0.4	29	–	–
	District roads	–	30	12.2	–	0.7	62	–	–
Benbow, Nesnas, and Wright [56]	Hampshire Route (UK)	43	430	0.63/0.34	–	–	–	–	–
Andrén [15]	Entire Swedish road network	–	–	~ 1.1	–	–	–	0.05	16.5
Nagel, Maerschalk, and Schneider [52]	Saarland (Germany)	2944	32 (26–100 km)	2.05	1.98	0.35	7.21	—	—
Kropáč and Múčka [53]	AC surfaces	2519.5	16,532	0.57	0.52	0.04	10.33	—	—
	PCC surfaces	1417	9,298	0.68	0.44	0.07	3.87	—	—
Múčka and Kropáč [59]	AC surfaces – full	2519.5	16,532	0.78	0.78	0.02	18.85	0.16	2.18
	AC surfaces – random part	2519.5	16,532	0.35	0.33	0.02	5.68	0.08	0.95
	PCC surfaces – full	1417	9,298	0.88	0.63	0.05	6.13	0.23	2.13
	PCC surfaces – random part	1417	9,298	0.44	0.32	0.03	4.15	0.1	1.1
Spielhofer et al. [55]	AC and PCC	115	30	1.51	1.32	0.27	5.37	–	–
	AC	47.3	14	1.85	1.5	0.53	5.37	–	–
	PCC	64.4	15	1.2	1.07	0.27	3.76	–	–
	Paved road	2.2	1	28.3	—	23.02	33.53	–	–
Kollmer, Kucukay, and Potter [51]	Highways, Germany	5602	11204	~ 5	—	—	—	0.5	30
	Highways, Eastern Europe	447	894	~ 5	—	—	—	0.2	25
	Highways, China	3350	6700	~ 5	—	—	—	0.3	22
	Extra urban roads, Germany	3284	6568	~ 5	—	—	—	0.5	70
	Extra urban roads, Eastern Europe	1872	3744	~ 8	—	—	—	0.7	80
	Extra urban roads, China	2175	4350	~ 12	—	—	—	7	100
	Urban roads, Germany	1114	2228	~ 20	—	—	—	2	115
	Urban roads, Eastern Europe	344	688	~ 25	—	—	—	2.5	400
	Urban roads, China	1211	2422	~ 25	—	—	—	5	270

A length of processed road network data was as follows: Andrén [15] – entire Swedish network, Nagel et al. [52] – 29,000 km, Kollmer et al. [51] – 20,000 km, Kropáč and Múčka [53] – 4,000 km, Braun and Hellenbroich [54] – 1,200 km, Spielhofer et al. [55] – 115 km and Benbow, Nesnas, and Wright [56] – 43 km. Nagel et al. [52] provided only unevenness index data. Only waviness was processed for Ducros et al. [57] and Maerschalk et al. [58] data.

Estimation of unevenness index is dependent on data processing conditions. Braun and Hellenbroich [54] and Nagel et al. [52] used a 100-m long section. Andrén [15] applied processing defined in ISO 8608 without smoothing in octave bands. The length of processed sections was not issued. Kropáč and Múčka [53] and Múčka and Kropáč [59] processed 152.4-m long LTPP sections. Kropáč and Múčka [53] used a narrower interval from 0.78 m to 50 m for fitting of raw PSD by a straight line. Múčka and Kropáč [59] processed the same test sections in a wavelength range from 0.35 to 90.9 m defined in ISO 8608. A pure random component of a road profile was separated from a raw profile based on a median filter method [60]. Spielhofer et al. [55] used a 1000-m long section. Data in Kollmer et al. [51] were fitted in narrower frequency band, Ω = 0.26–9 rad/m (i.e., L = 0.7–24 m) in comparison to ISO 8608.

Table 4 shows that a similar level of unevenness index was calculated for highways in Germany, the United States, the UK, Japan, and Sweden [15,52–56,59,61]. Mean values for these profiles correspond to road class A.

Worst-quality roads based on maximum value or P95 value correspond to A or B class [51–55,59,61] or mean value of C class [15]. Country or district roads can be rated to B or C class and worst-quality roads can be rated a D class [54].

Kollmer et al. [51] obtained higher values of unevenness index for a large amount of a road network. Mean values for highways and extra urban roads can be rated a B class and for urban roads a C class. Worst-quality urban or extra urban roads can be rated a D or E class.

The spread of unevenness index for urban roads does not exceed $G_d(\Omega_0) = 100 \times 10^{-6}$ m^3/rad for German roads [51]. Some sections in China roads were identified to be of 270×10^{-6} m^3/rad and in Eastern Europe roads to be of 400×10^{-6} m^3/rad. These values correspond to results obtained by Wandeborn [62] for country roads (24×10^{-6} m^3/rad) or for a track across a field (180×10^{-6} m^3/rad). Braun and Hellenbroich [54] identified the similar extent for country roads ($5.3–29 \times 10^{-6}$ m^3/rad) and district roads ($12.2–62 \times 10^{-6}$ m^3/rad). Braun and Hellenbroich [54] identified for unpaved road of good quality 31.8×10^{-6} m^3/rad and of average quality 155×10^{-6} m^3/rad. Paraforos et al. [63] identified a country road to be a class D with $w = 2.66$ and 2.51 for parallel profiles and a field profile to be classes D and E with $w = 2.4$ and 2.2.

Reasons for a higher unevenness index in Kollmer et al. [51] were difficult to identify in comparison to other sources. Road data pre-processing and spectrum fitting conditions were only briefly described. Kollmer et al. [51] fitted a raw spectrum in narrower frequency band, $\Omega = 0.26–9$ rad/m ($L = 0.7–24$ m) in comparison to ISO 8608 that defined a band, $L = 0.3534–90.9$ m. Further, the authors used their own measurement system that consisted of one laser sensor and two acceleration sensors for each wheel track.

In Germany, unevenness index values $G_d(\Omega_0) = 1$, 3, and 9×10^{-6} m^3/rad respectively are fixed for the target, warning and threshold values on long-distance highways [58,64]. This means that a B class upper limit is considered to be the threshold value for highways.

Waviness of Real Road Sections

Table 5 presents statistics of calculated waviness based on 9 different sources. For data in Andrén [15] and Kollmer et al. [51], waviness was roughly estimated from figures.

Estimation of waviness is a function of data processing conditions. Braun and Hellenbroich [54] and Mearschalk et al. [58] used a 100-m long section. Waviness data were roughly estimated from figures of measured road PSD in Ducros et al. [57].

Andrén [15], Braun and Hellenbroich [54], Kropáč and Múčka [53], Múčka and Kropáč [59], Kollmer et al. [51], Ducros et al. [57], and Maerschalk et al. [58] identified mean waviness, $w > 2$. Mean value, $w \sim 2$, was calculated for better-quality roads such as freeways or highways [51,54].

Kollmer et al. [51] stated that waviness, $w = 2$, presents an appropriate approximation for highways. For extra urban roads, the average waviness value was ~ 2.4 for China roads and ~ 1.9 for German roads. Differences arose due to the many concrete surfaces in the group of China roads. Mean waviness for urban roads in China, Eastern Europe and Germany roads was similar, $w \sim 2.6$.

The processing of Portland cement concrete (PCC) surfaces showed lower values of waviness in comparison to asphalt concrete (AC) surfaces. Differences in mean waviness ($\Delta w = w_{PCC} - w_{AC}$) based on road surface type were identified as follows: $\Delta w = –0.35$ [54], –0.2 [55], –0.08 [58], –0.05 [59]. A decrease in mean waviness may be caused by increased wavelength contents in the short-wave band for angular spatial frequencies $\Omega > 1$ rad/m (i.e., $L < 6.28$ m). Short-wave content is influenced by the presence of local distresses or joints in PCC surfaces. Higher mean waviness was identified for local roads in comparison to highways. Mean waviness, $w = 2.3–2.4$, was calculated for country and district roads [54], ~ 2.6 for urban roads [51] or ~ 2.6 for federal roads [58]. Waviness could be roughly estimated to be in a range from 1 to 3.5.

Standard proposal prEN 13 036-5 [16] uses waviness $w = 2.6$ for a reference spectrum intended for Weighted Longitudinal Profile (WLP) calculation [64].

The BSI proposal [14] used two different waviness values (Eq 2) based on processing of 53 test sections [13]. Andrén [15], Kropáč and Múčka [53], Múčka and Kropáč [59], or Múčka [65] confirmed different spectrum slope in long- and short-wave bands. Andrén [15] calculated $w_1 \sim 2.9$ and $w_2 \sim 1.2$ for $\Omega_0 = 5.15$ rad/m. Kropáč and Múčka [53] calculated $w_1 = 3.22$ and $w_2 = 2.09$ for AC pavements and $w_1 = 2.43$ and $w_2 = 2.38$ for PCC pavements and $\Omega_0 = 1$ rad/m. Múčka [65] obtained $w_1 = 2.38$ and $w_2 = 1.38$ for $\Omega_0 = 3.46$ rad/m and unconnected line segments.

The influence of waviness of simulated roads on vibration response was analyzed in [66,57] for two longitudinal half-car vehicle models, the influence of unevenness index and waviness calculated for real road sections on a half-car model in Múčka [68] and Múčka and Gagnon [69] and on a real truck in Múčka and Gagnon [69]. Múčka [50] presented a proposal of road classification based on spectrum parameters of real roads and an induced vibration response on a passenger car model.

Table 5. Statistics of waviness of real road sections.

Source	Road surface type/ Road functional category	Length (km)	Number of sections	*w*					
				mean	std	min	max	P5	P95
Kawamura and Kaku [61]	Various – Summer	—	10	1.73	0.47	1.29	2.75	—	—
	Various – Winter	—	10	1.46	0.90	0.87	3.67	—	—
Braun and Hellenbroich [54]	Various	1282.0	12820	2.14	0.29	1.94	2.94	1.67	2.55
	AC surfaces	882.5	8826	2.20	0.22	1.63	2.94	1.88	2.60
	PCC surfaces	399.4	3994	1.85	0.17	1.49	2.55	1.65	2.12
	Highways	—	240	2.0	—	1.5	2.6	—	—
	Federal roads	—	70	2.3	—	1.7	2.9	—	—
	Country roads	—	35	2.4	—	1.9	2.9	—	—
	District roads	—	30	2.3	—	1.8	2.9	—	—
Ducros et al. [57]	Various types	—	44	2.49	0.40	1.87	3.90	—	—
Andrén [15]	Entire Swedish road network	—	N/A	~ 2.3	~ 0.3	~ 1.4	~ 3.2	—	—
Kropáč and Múčka [53]	AC surfaces	2519.5	16532	2.47	0.42	1.13	4.82	—	—
	PCC surfaces	1417	9298	2.48	0.31	0.84	4.65	—	—
Múčka and Kropáč [59]	AC surfaces – full	2519.5	16532	2.86	0.22	2.2	4.17	2.54	3.25
	AC surfaces – random	2519.5	16532	2.75	0.36	1.34	4.3	2.15	3.31
	PCC surfaces - full	1417	9298	2.81	0.18	2.27	3.99	2.52	3.11
	PCC surfaces - random	1417	9298	2.71	0.3	1.2	4.09	2.17	3.17
Spielhofer et al. [55]	AC	47.3	14	2.55	0.07	2.42	2.68	—	—
	PCC	64.4	15	2.35	0.08	2.19	2.48	—	—
	Paved road	2.2	1	2.41	—	2.38	2.44	—	—
	AC/PCC	115	30	2.45	0.12	2.19	2.68	—	—
Kollmer, Kucukay, and Potter [51]	Highways, Germany	5602	11204	~ 2	—	—	—	1.24	2.63
	Highways, Eastern Europe	447	894	~ 2	—	—	—	1.28	2.66
	Highways, China	3350	6700	~ 1.9	—	—	—	1.11	2.97
	Extra urban roads, Germany	3284	6568	~ 1.9	—	—	—	0.93	2.76
	Extra urban roads, Eastern Europe	1872	3744	~ 2	—	—	—	0.97	3.08
	Extra urban roads, China	2175	4350	~ 2.4	—	—	—	1.37	3.13
	Urban roads, Germany	1114	2228	~ 2.6	—	—	—	1.48	3.33
	Urban roads, Eastern Europe	344	688	~ 2.6	—	—	—	1.47	3.42
	Urban roads, China	1211	2422	~ 2.6	—	—	—	1.55	3.31
Maerschalk, Ueckermann, and Heller [58]	Highways – AC+PCC surfaces	5237.19	523719	2.22	—	—	—	—	—
	Highways – AC	3878.44	387844	2.24	—	—	—	—	—
	Highways – PCC surfaces	1358.43	135843	2.16	—	—	—	—	—
	Bundesstrassen – AC+PCC surfaces	7325.11	732511	2.60	—	—	—	—	—
	Bundesstrassen – AC	7265.12	726512	2.60	—	—	—	—	—
	Bundesstrassen – PCC surfaces	25.20	2520	2.14	—	—	—	—	—

Correlation between Unevenness Index and Waviness

Spectrum parameters make it possible to compare correlation. Table 6 presents fitting parameters of the relation $G_d(\Omega_0) = f(w)$. Fitting parameters were calculated for published data [53–55,59,61] or were roughly estimated from figures presented in [15] and [51].

On average, w follows $G_d(\Omega_0)$ according to formula

$$\log(G_d(\Omega_0)) = b_1 w + b_2 \tag{10}$$

where b_1 is a linear term and b_2 is an intercept. Linear relation (Eq. 10) was introduced based on the tendency of observed data of $\log(G_d(\Omega_0))$ relation on w presented in Andrén [15] or Kollmer et al. [51] for urban and extra urban roads. The unevenness index slightly increased with waviness. The linear term b_1 varies from 0.45 to 2.5. A weak correlation was often observed between $\log(G_d(\Omega_0))$ and w. The coefficient of determination R^2 ranged from 0.04 to 0.449 for a larger sample size [15,51,54,55,59] and was 0.656 and 0.975 for a smaller sample size [61]. Calculated R^2-values mostly indicated weak strength in the linear

component b_1 of the model (Eq 10). Low values of R^2 reflect the reality. Processed road sections are of different road functional categories, age, construction, or traffic load. Group of road sections with similar properties shows higher values of R^2.

Processing the data of Kawamura and Kaku [61] showed a decrease in the unevenness index with waviness for summer measurements and an increase for winter measurements. Estimations of b_1 and b_2 for Kawamura and Kaku [61] and Spielhofer et al. [55] have a much higher relative error in comparison to other data.

Similar slope b_1 was obtained for data published in Andrén [15], Braun and Hellenbroich [54], Múčka and Kropáč [59], and Kollmer et al. [51]. Higher slope was obtained for data in Spielhofer et al. [55]. This could be caused by use of a higher interval (1000 m) for evaluation.

An increase of $\log(G_d(\Omega_0))$ with w may be interpreted that for lower-quality roads the long-wave content is prevalent. This may be caused by an interaction of a vehicle fleet with a road profile. Longer waves ($\Omega_0 < 1$ rad/m, $L_0 > 6.28$ m) may excite resonance frequencies (~ 0.8–1.5 Hz) of vehicle sprung masses, i.e., car body. Sprung masses have a much greater weight than unsprung masses (axle, tire) and can cause higher dynamic forces to the pavement. The interaction of a vehicle fleet with a road profile can cause an increase in long-wave content.

According to Kollmer et al. [51], urban and extra urban roads seem to have some kind of dependency between the unevenness index and waviness. This correlation was most clear on urban and extra urban roads. Kollmer et al. [51] roughly estimated a linear term for Eq 10 to be $b_1 \sim 1$. It seems according to corresponding figures in [51] that the value of b_1 could be lower.

Andrén [15] suggested a correlation between the roughness level and waviness for a straight line fit. The linear term b_1 was roughly estimated to be from 0.8–1.2.

Table 6. Fitting parameters of relation $\log(G_d(\Omega_0)) = b_1 w + b_2$ (Eq 10).

Reference	Road surface type/ Road functional category	b_1	std(b_1)	b_2	std(b_2)	rmse	R^2
Kawamura and Kaku [61]	Various – summer	-1.09	1.11	1.52	1.55	0.355	0.656
	Various – winter	0.674	0.273	-1.06	0.994	1.46	0.975
Braun and Hellenbroich [54]	AC	0.758	0.070	-1.44	0.17	0.758	0.040
	PCC	0.900	0.051	-1.54	0.10	1.460	0.133
Andrén [15]	AC + PCC	0.7–1.2	–	–	–	–	0.449
Múčka and Kropáč [59]	AC	0.314	0.018	-0.985	0.052	0.751	0.252
	PCC	0.466	0.018	-1.34	0.053	0.563	0.442
	AC – random part	0.676	0.019	-2.41	0.057	0.300	0.192
	PCC – random part	0.641	0.025	-2.18	0.074	0.290	0.183
Spielhofer et al. [55]	AC	1.36	3.23	-3.20	8.30	1.460	0.053
	PCC	2.51	3.45	-5.87	8.29	0.945	0.222
Kollmer, Kucukay, and Potter [51]	Highways (Germany, Eastern Europe, China)	0.6, 0.45, 0.55	—	—	—	—	—
	Extra urban roads (Germany, Eastern Europe, China)	0.5, 0.5, 0.6	—	—	—	—	—
	Urban roads (Germany, Eastern Europe, China)	0.6, 0.7, 0.8	—	—	—	—	—

Conclusions

Imprudent use of road profiles based on road classes specified in ISO 8608 may lead to excessive expectations and unrealistic results. Differences were observed between simulated road profiles based on road classes used in scientific literature and the spectrum content of real roads. A sample of 27 current scientific papers that used ISO 8608 road classes were compared with spectrum parameters of real roads based on eleven sources.

(1) Based on a review of published results, A and B classes may be roughly recommended as a representative of a typical road profile that correspond to road functional categories such as motorways, expressways or first class roads. Mean values of highway profiles measured in various countries correspond to road class A [15,52–56,59,61]. Worst-quality roads based on a maximum value or P95 value correspond to A or B class [52–55,59,61] or a mean value of a C class [15]. Country or district roads can be approximated by B or C class [54].

(2) Road classes D to H often correspond to unpaved roads. Velocities used for such profiles should reflect a poor smoothness quality. About 41% of the investigated sample of 27 scientific papers used class D or higher classes. Only some authors adjusted the vehicle speed for this fact.

(3) Simulation of vehicle model response with considering ride safety and ride comfort thresholds has shown that recommended maximum velocities would be > 100 km/h for class A and B, 30–60 km/h for class C and < 15 km/h for class D.

(4) Identified waviness differs from the $w = 2$ that is used in the ISO 8608. Many authors identified a mean waviness $w > 2$ [15,51,53,54,57–59]. The mean value $w \sim 2$ was calculated for roads of better quality such as highways [51,54]. To model a good quality roads (highways, expressways), waviness $w = 2$ may be recommended. To model a primary and secondary road of lower quality the value $w = 2–2.6$ may be recommended. Processing of PCC surfaces showed lower values of waviness in comparison to AC surfaces.

(5) The unevenness index slightly increased with waviness. A weak correlation was often observed between unevenness index and waviness.

(6) Some authors still used an older version of ISO standard [14] with an approximation of road profile spectrum with two straight-lines. This standard proposal was based on 45-year-old measurements of a limited sample of 53 sections.

Acknowledgement

This work was supported by the VEGA Grant Agency of the Slovak Academy of Sciences under Grant No. 2/0089/16.

References

[1] ISO 8608: Mechanical Vibration–Road Surface Profiles–Reporting of Measured Data, International Standardization Organization, Geneva, Switzerland, 1995.

[2] Johannesson, P. and Rychlik, I., "Modelling of Road Profiles Using Roughness Indicators," *Int. Journal of Vehicle Design*, Vol. 66, No. 4, 2014, pp. 317–346.

[3] Johannesson, P., Podgórski, K., and Rychlik, I., "Modelling Roughness of Road Profiles on Parallel Tracks Using Roughness Indicators," *Int. Journal of Vehicle Design*, Vol. 70, No. 2, 2016, pp. 183–210.

[4] Davis, B. R. and Thompson, A. G., "Power Spectral Density of Road Profiles," *Veh. Syst Dyn.*, Vol. 35, No. 6, 2001, pp. 409–415.

[5] Steinwolf, A., "Vibration Testing by Non-Gaussian Random Excitations with Specified Kurtosis. Part I: Discussion and Methods," *J. Test. Eval.,* Vol. 42, No. 3, 2014, pp. 659–671.

[6] Steinwolf, A., "Vibration Testing by Non-Gaussian Random Excitations with Specified Kurtosis. Part II: Numerical and Experimental Results," *J. Test. Eval.,* Vol. 42, No. 3, 2014, pp. 672–686.

[7] Dunno, K. and Batt, G. S., "Experimental Comparison of Vehicle Vibration Simulation Techniques," *J. Test. Eval.*, Vol. 44, No. 6, 2016.

[8] Rouillard, V., Sek, M. A. and Bruscella, B., "Simulation of Road Surface Profiles," *J. Transp. Eng.*, Vol. 127, No. 3, 2001, pp. 247–253.

[9] Rouillard, V. and Sek, M. A., "The Simulation of Nonstationary Vehicle Vibrations," *Proceedings of the Institution of Mechanical Engineers – Part D: Journal of Automobile Engineering,* Vol. 215, No. 10, 2001, pp. 1069–1075.

[10] Rouillard, V. and Sek, M. A., "Synthesizing Nonstationary, Non-Gaussian Random Vibrations," *Packaging Technology and Science*, Vol. 23, No. 8, 2010, pp. 423–439.

[11] Rouillard, V., "Decomposing Pavement Surface Profiles Into a Gaussian Sequence," *Int. J. Veh. Systems Model. Test.*, Vol. 4, No. 4, 2009, pp. 288–305.

[12] Braun, H., "Untersuchungen über Fahrbahnunebenheiten und Anwendung der Ergebnisse," [Studies on uneven road surfaces and application of results], *Deutsche Kraftfahrtforschung und Strassenverkehrstechnik*, Heft 186, 1966.

[13] La Barre, R. P., Forbes, R. T., and Andrews, S., "The Measurement and Analysis of Road Surface Roughness," *Report No 1970/5*, Motor Industry Research Association, 1970.

[14] BSI MEE/158/3/1, Proposals for Generalised Road Inputs to Vehicles, British Standard Institution (BSI), London, BSI 72/34562, 1972.

[15] Andrén, P., "Power Spectral Density Approximations of Longitudinal Road Profiles," *Int. J. Veh. Des.*, Vol. 40, Nos. 1/2/3, 2006, pp. 2–14.

[16] prEN 13036-5: Road and Airfield Surface Characteristics – Test Methods, Part 5: Determination of Longitudinal Unevenness Indices, European Committee for Standardization (CEN), Brussels, Belgium, 2015.

[17] Dodds, C. J. and Robson, J. D., "The Description of Road Surface Roughness," *J. Sound Vib.*, Vol. 31, No. 2, 1973, pp. 175–183.
[18] Robson, J. D., "Road surface description and vehicle response," *Int. J. Veh. Des.*, Vol. 1, No. 1, 1979, pp. 25–35.
[19] Aied, H., González, A., and Cantero, D., "Identification of sudden stiffness changes in the acceleration response of a bridge to moving loads using ensemble empirical mode decomposition," *Mechanical Systems and Signal Processing*, Vol. 66–67, 2016, pp. 314–338.
[20] Shen, Y., Chen, L., Yang, X., Shi, D., and Yang, J., "Improved design of dynamic vibration absorber by using the inerter and its application in vehicle suspension," *J. Sound Vib.*, Vol. 361, 2016, 148–158.
[21] Ataei, M., Asadi, E., Goodarzi, A., Khajepour, A., and Khamesee, M. B., "Multi-objective optimization of a hybrid electromagnetic suspension system for ride comfort, road holding and regenerated power," *Journal of Vibration and Control*, 2016, doi: 10.1177/1077546315585219 (in press).
[22] Xie, X. D. and Wang, Q., "Energy Harvesting from a Vehicle Suspension System," *Energy*, Vol. 86, 2015, pp. 385–392.
[23] Prendergast, L. J., Hester, D., and Gavin, K., "Development of a Vehicle-Bridge-Soil Dynamic Interaction Model for Scour Damage Modelling," *Shock and Vibration*, 501, 2015, Art. Number 935693.
[24] Huang, B., Hsieh, Ch.-Y., Golnaraghi, F., and Moallem, M., "Development and optimization of an energy-regenerative suspension system under stochastic road excitation," *J. Sound Vib.*, Vol. 357, 2015, pp. 16–34.
[25] Drehmer, L. R. C., Paucar Casas, W. J., and Gomes, H. M., "Parameters optimisation of a vehicle suspension system using a particle swarm optimisation algorithm," *Veh. Syst Dyn.*, Vol. 53, No. 4, 2015, pp. 449–474.
[26] Xiao, L. and Zhu, Y., "Sliding-mode output feedback control for active suspension with nonlinear actuator dynamics," *Journal of Vibration and Control*, Vol. 21, No. 14, 2015, pp. 2721–2738.
[27] Wang, W., Song, Y., Xue, Y., Jin, H., Hou, J., and Zhao, M., "An optimal vibration control strategy for a vehicle's active suspension based on improved cultural algorithm," *Applied Soft Computing*, Vol. 28, 2015, pp. 167–174.
[28] Zhang, Y., Cai, C. S., and Deng, L., "Piezoelectric-based energy harvesting in bridge systems," *Journal of Intelligent Material Systems and Structures*, Vol. 25, No. 12, 2014, pp. 1414–1428.
[29] Reza-Kashyzadeh, K., Ostad-Ahmad-Ghorabi, M. J., and Arghavan, A., "Investigating the effect of road roughness on automotive component," *Engineering Failure Analysis*, Vol. 41, 2014, pp. 96–107.
[30] Jaksic, V., O'Connor, A., and Pakrashi, V., "Damage detection and calibration from beam–moving oscillator interaction employing surface roughness." *J. Sound Vib.*, Vol. 333, No. 17, 2014, pp. 3917–3930.
[31] Zhou, Q., Li, B., Kuang, Z., Xie, D., Tong, G., Hu, L., and Yuan, X., "A quarter-car vehicle model based feature for wheeled and tracked vehicles classification," *J. Sound Vib.*, Vol. 332. No. 26, 2013, pp. 7279–7289.
[32] Oliva, J., Goicolea, J. M., Antolín, P., and Astiz, M. Á., "Relevance of a complete road surface description in vehicle–bridge interaction dynamics," *Engineering Structures*, Vol. 56, 2013, pp. 466–476.
[33] Shiiba, T., Obana, K., and Machida, N., "Comparison of Linearized vs. Non-linearized Multibody Vehicle Model for Real-Time Simulation," *Int. Journal of Non-Linear Mechanics*, Vol. 53, 2013, pp. 32–40.
[34] Zuo, L. and Zhang, P.-S., "Energy harvesting, ride comfort, and road handling of regenerative vehicle suspensions," *Journal of Vibration and Acoustics*, Vol. 135, No. 1, 2013, Art. Number 011002. pp. 1–8.
[35] Li, Y., Sun, W., Huang, J., Zheng, L., and Wang, Y., "Effect of Vertical and Lateral Coupling Between Tyre and Road on Vehicle Rollover," *Veh. Syst Dyn.* , Vol. 51, No. 8, 2013, pp. 1216–1241.
[36] Zhang, G., Cao, J., and Yu, F., "Design of active and energy-regenerative controllers for DC-motor-based suspension," *Mechatronics,* Vol. 22, No. 8, 2012, pp. 1124–1134.
[37] González, A., O'Brien, E. J., and McGetrick, P. J., "Identification of damping in a bridge using a moving instrumented vehicle," *J. Sound Vib.*, Vol. 331, No. 18, 2012, pp. 4115–4131.
[38] Chang, K. C., Wu, F. B. and Yang, Y. B., "Disk model for wheels moving over highway bridges with rough surfaces," *J. Sound Vib.*, Vol. 330, No. 20, 2011, pp. 4930–4944.
[39] Harris, N. K., González, A., O'Brien, E. J., and McGetrick, P., "Characterisation of pavement profile heights using accelerometer readings and a combinatorial optimisation technique," *J. Sound Vib.*, Vol. 329, No. 5, 2010, pp. 497–508.
[40] González, A., O'Brien, E. J., Cantero, D., Li, Y., Dowling, J., and Žnidarič, A., "Critical speed for the dynamics of truck events on bridges with a smooth road surface," *J. Sound Vib.*, Vol. 329, No. 11, 2010, pp. 2127–2146.
[41] Ding, L., Hao, H., and Zhu, X., "Evaluation of dynamic vehicle axle loads on bridges with different surface conditions," *J. Sound Vib.*, Vol. 323, No. 3–5, 2009, pp. 826–848.
[42] Xu, Y. L. and Hong, X. J., "Stochastic modelling of traffic-induced building vibration," *J. Sound Vib.*, Vol. 313, No. 1–2, 2008, pp. 149–170.
[43] Yarmohamadi, H. and Berbyuk, V., "Kinematic and dynamic analysis of a heavy truck with individual front suspension," *Veh. Syst Dyn.*, Vol. 51, No. 6, 2013, pp.877–905.
[44] Chen, X., Ma, R., and Yang, J., "Dynamic attributions of pavement unevenness by full-vehicle model simulation," *J. Test. Eval.*, Vol. 44, No. 2, 2016, pp. 820–826.
[45] Reina, G. and Delle Rose, G., "Active vibration absorber for automotive suspensions: a theoretical study," *Int. J. Heavy Vehicle Systems*, Vol. 23, No. 1, 2016, pp. 21–39.
[46] Yu, S., Wang, F., Wang, J. and Chen, H., "Full-car active suspension based on H2/generalised H2 output feedback control," *Int. J. Veh. Des.*, Vol. 68, Nos. 1/2/3, 2015, pp. 37–54.

[47] Sayers, M. W., Gillespie, T. D., and Paterson, W. D. O., "Guidelines for Conducting and Calibrating Road Roughness Measurements," *Technical Paper No. 46*, The World Bank, Washington, DC, USA, 1986.
[48] ISO 2631-1: Mechanical Vibration and Shock–Evaluation of Human Response to Whole Body Vibration. Part I: General Requirements, International Standardization Organization, Geneva, Switzerland, 1997.
[49] Cebon, D. "Handbook of Vehicle-Road Interaction," Swets & Zeitlinger, Lisse, the Netherlands, 1999, 616 p.
[50] Múčka, P., "Proposal of road unevenness classification based on the road elevation spectrum parameters," *J. Test. Eval.*, Vol. 44, No. 2, 2016, pp. 930–944.
[51] Kollmer, H., Kucukay, F., and Potter, K., "Measurement and fatigue damage evaluation of road profiles in customer operation," *Int. J. Veh. Des.*, Vol. 56, Nos. 1/2/3/4, 2011, pp. 106–124.
[52] Nagel, M., Maerschalk, G., and Schneider, B., "Variabilitätsuntersuchung der Rohdaten zur Stabilisierung der Ableitung abschnittsbezogener Zustandsgrößen für die Bewertung der Fahrbahnbefestigungen der Bundesfernstraßen," [Variability analysis of the raw data for the stabilization of the derivative section related state variables for evaluating the pavements of the federal roads], *Projekt-Nr. 29.0178/2007/BMVBS*, SAP Maerschalk, Munchen, Germany, 2008, 61 p.
[53] Kropáč, O. and Múčka, P., "Indicators of longitudinal unevenness of roads in the USA," *Int. J. Veh. Des.*, Vol. 46, No. 4, 2008, pp. 393–415.
[54] Braun, H. and Hellenbroich, T., *Results of road roughness measurement in Germany*, VDI-Berichte Nr. 877, VDI-Verlag, Düsseldorf, Germany, 1991, pp. 47–80.
[55] Spielhofer, R., Brozek, B., Maurer, P., Fruhmann, G., and Reinalter, W., "Development of a parameter for evaluating longitudinal evenness," *Straßenforschung Nr. 3.301*, Vol. 582, 2009, pp. 1–152 (in German).
[56] Benbow, E., Nesnas, K., and Wright, A., *Shape (surface form) of local roads*, Transport Research Laboratory Limited, Wokingham, UK, 2006, 99 p.
[57] Ducros, D. M., Petkovic, L., Descornet, G., Berlemont, B., Alonso Anchuelo, M., Yanguas, S., Jendryka, W., and Andrén, P., "Filter Experiment – Longitudinal Analysis," *FEHRL Final Rep. 2001/1*, Laboratoire Central des Ponts et Chausses, Paris, France, 2001.
[58] Maerschalk, G., Ueckermann, A., and Heller, S., "Längsebenheitsauswerteverfahren "Bewertetes Längsprofil": Weiterentwicklung der Längsebenheitsbewertung der Zustandserfassung und –Bewertung," [Analysis procedure for longitudinal road roughness "Weighted Longitudinal Profile"], *Berichte der Bundesanstalt für Straßenwesen, Reihe S: Straßenbau*, *Heft S73*, Bergisch Gladbach, Germany, 2011.
[59] Múčka, P. and Kropáč, O., "Properties of random component of longitudinal road profile influenced by local obstacles," *Int. J of Vehicle Systems Modelling and Testing*, Vol. 4, No. 4, 2009, pp. 256–276.
[60] Kropáč, O. and Múčka, P., "Specification of obstacles in the longitudinal road profile by median filtering," *J. Transp. Eng.*, Vol. 137, No. 3, 2011, pp. 214–226.
[61] Kawamura, A. and Kaku, T., "An evaluation of road roughness and the effects on riding comfort and vehicle dynamics," *Proc. of JSCE*, Vol. 359, 1985, pp. 137–147.
[62] Wandeborn, J. O., "Die Unebenheiten landwirtschaftlicher Fahrbahnen als Schwingungserreger landwirtschaftlicher Fahrzeuge," [The unevenness of agricultural roads as vibration excitation source of agricultural vehicles] , *Grundlagen der Landtechnik*, Vol. 15, No. 2, 1965, pp.33–46.
[63] Paraforos, D. S., Griepentrog, H. W., and Vougioukas, S. G., "Country road and field surface profiles acquisition, modelling and synthetic realisation for evaluating fatigue life of agricultural machinery," *Journal of Terramechanics*, Vol. 63, 2016, pp. 1–12.
[64] Ueckermann, A. and Steinauer, B., "The weighted longitudinal profile. A new method to evaluate the longitudinal evenness of roads," *Road Materials and Pavement Design*, Vol. 9, No. 2, 2008, pp. 135–157.
[65] Múčka, P., "Longitudinal road profile spectrum approximation by split straight lines," *J. Transp. Eng.*, Vol. 138, No. 2, 2012, pp.243–251.
[66] Kropáč, O. and Múčka, P., "Effect of obstacles on roads with different waviness values on the vehicle response," *Veh. Syst Dyn.*, Vol. 46, No. 3, 2008, pp. 155–178.
[67] Kropáč, O. and Múčka, P., "Effects of longitudinal road waviness on vehicle vibration response," *Veh. Syst Dyn.*, Vol. 47, No. 2, 2009, pp.135–153.
[68] Múčka P., "Correlation among road unevenness indicators and vehicle vibration response," *J. Transp. Eng.*, Vol. 139, No. 8, 2013, pp.771–786.
[69] Múčka, P. and Gagnon, L., "Influence of tyre-road contact model on vehicle vibration response," *Veh. Syst Dyn.*, Vol. 53, No. 9, 2015, pp. 1227–1246.

FIGURES

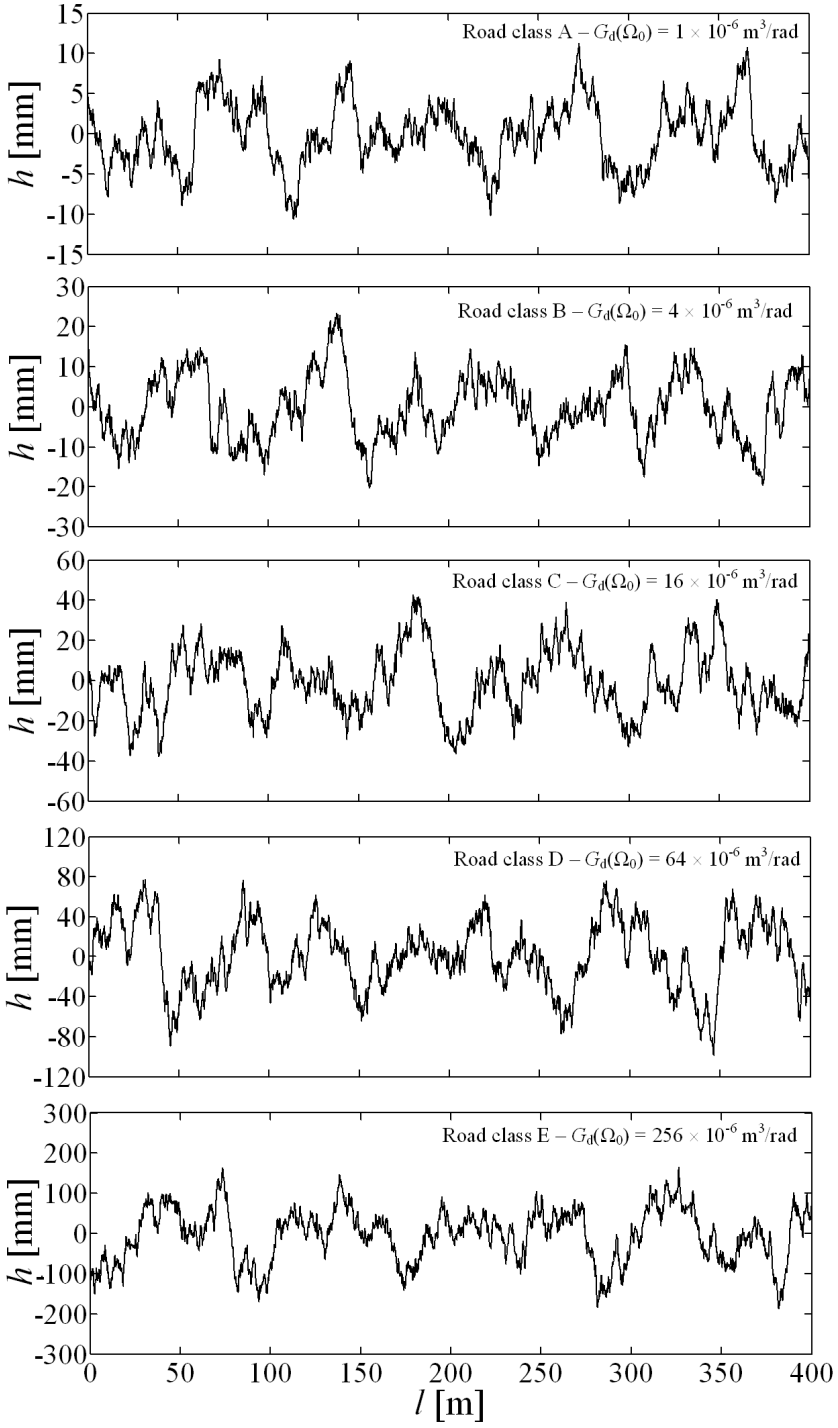
Road class A – $G_d(\Omega_0)$ = 1 × 10^{-6} m^3/rad
Road class B – $G_d(\Omega_0)$ = 4 × 10^{-6} m^3/rad
Road class C – $G_d(\Omega_0)$ = 16 × 10^{-6} m^3/rad
Road class D – $G_d(\Omega_0)$ = 64 × 10^{-6} m^3/rad
Road class E – $G_d(\Omega_0)$ = 256 × 10^{-6} m^3/rad
h [mm]
l [m]

(a)

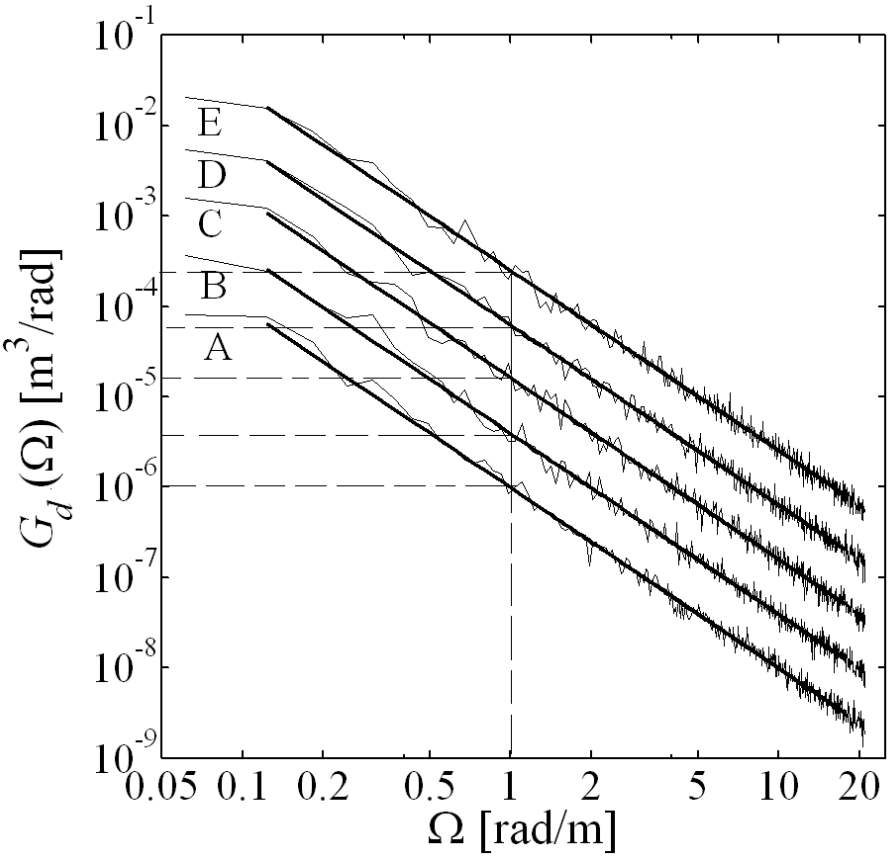

(b)

FIG. 1. Simulated road profiles characterized by unevenness index $G_d(\Omega_0)$ = 1, 4, 16, 64, and 256 × 10^{-6} m^3/rad: (a) longitudinal road profile elevation; (b) road profile elevation PSD.

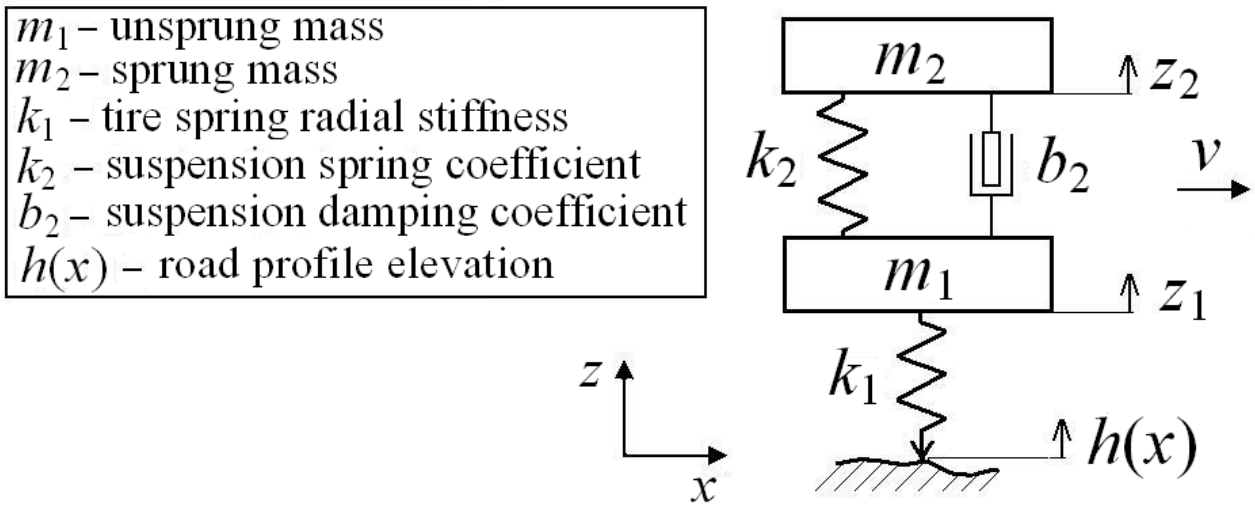

FIG. 2. The quarter-car model.

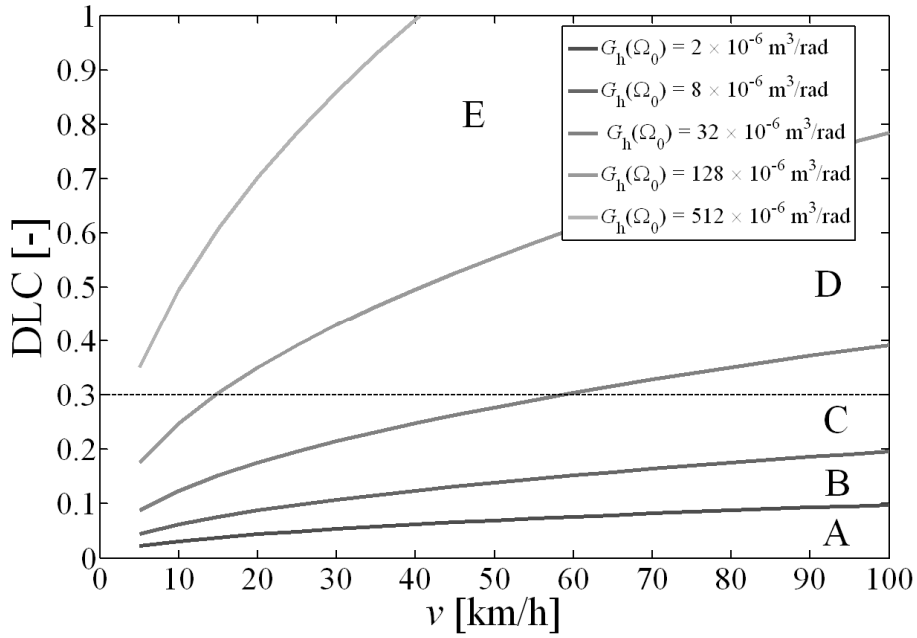

(a)

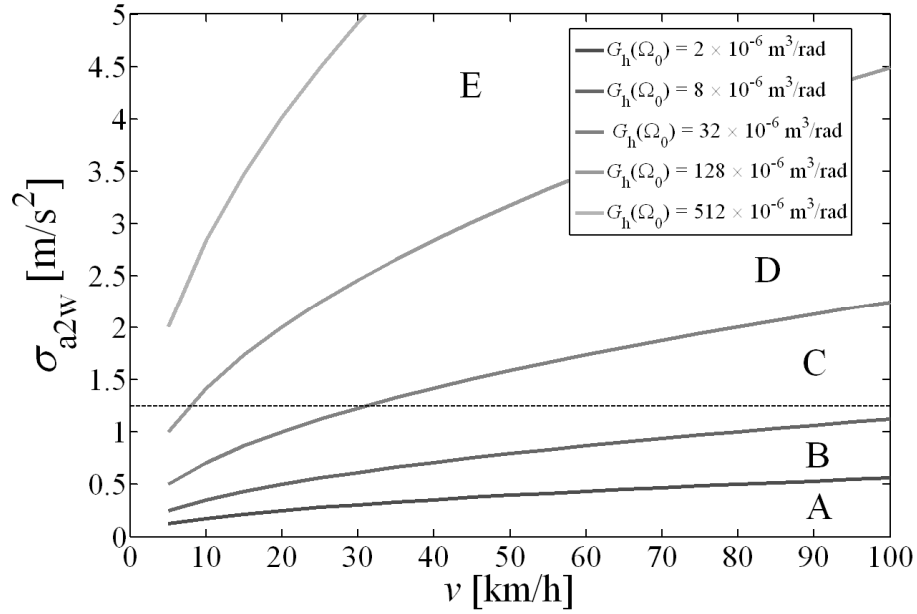

(b)

FIG. 3. Vibration response as a function of ISO 8608 road class and vehicle model velocity: (a) RMS value of frequency-weighted acceleration of the sprung mass, σ_{a2w}; (b) dynamic load coefficient, DLC.